PCCP

Electron Confinement Meet Electron Delocalization: Non-Additivity and Finite-Size Effects in the Polarizabilities and Dispersion Coefficients of the Fullerenes

Journal:	*Physical Chemistry Chemical Physics*
Manuscript ID	CP-ART-10-2020-005638.R1
Article Type:	Paper
Date Submitted by the Author:	07-Jan-2021
Complete List of Authors:	Lao, Ka Un; Cornell University Yang, Yan; Cornell University DiStasio Jr., Robert; Cornell University

Electron Confinement Meet Electron Delocalization: Non-Additivity and Finite-Size Effects in the Polarizabilities and Dispersion Coefficients of the Fullerenes

Ka Un Lao,[1,*] Yan Yang,[1,*] and Robert A. DiStasio Jr.[1,†]

[1] *Department of Chemistry and Chemical Biology, Cornell University, Ithaca, NY 14853 USA*

(Dated: January 14, 2021)

In this work, we used finite-field derivative techniques and density functional theory (DFT) to compute the static isotropic polarizability series (α_ℓ with $\ell = 1, 2, 3$) for the C_{60}–C_{84} fullerenes and quantitatively assess the intrinsic non-additivity in these fundamental response properties. By comparing against classical models of the fullerenes as conducting spherical shells (or solid spheres) of uniform electron density, a detailed critical analysis of the derived effective scaling laws ($\alpha_1 \sim N^{1.2}$, $\alpha_2 \sim N^{2.0}$, $\alpha_3 \sim N^{2.7}$) demonstrates that the electronic structure of finite-sized fullerenes—a unique dichotomy of electron confinement and delocalization effects due to their quasi-spherical cage-like structures and encapsulated void spaces—simultaneously limits *and* enhances their quantum mechanical response to electric field perturbations. Corresponding frequency-dependent polarizabilities were obtained by inputting the α_ℓ series into the hollow sphere model (within the modified single frequency approximation), and used to compute the molecular dispersion coefficients (C_n with $n = 6, 8, 9, 10$) needed to describe the non-trivial van der Waals (vdW) interactions in fullerene-based systems. Using first-order perturbation theory in conjunction with $>140,000$ DFT calculations, we also computed the non-negligible zero-point vibrational contributions to α_1 in C_{60} and C_{70}, thereby enabling a more accurate and direct comparison between theory and experiment for these quintessential nanostructures.

INTRODUCTION

The molecular polarizability (α_ℓ) describes the tendency of a molecule to form an induced multipole moment in the presence of an electric field (α_1, dipole polarizability), field gradient (α_2, quadrupole polarizability), field Laplacian (α_3, octupole polarizability), and/or higher field derivatives.[1–4] Knowledge of the α_ℓ series is crucial when describing induction and dispersion/vdW interactions,[4–6] predicting/understanding the spectroscopic signatures (*i.e.*, Raman, sum-frequency generation) of molecules and condensed matter,[7,8] as well as developing next-generation polarizable force fields and machine-learning based intra-/inter-molecular potentials. As quantum mechanical response properties, the α_ℓ series is governed by complex many-body interactions (*e.g.*, electron correlation, charge delocalization, secondary polarization), and tends to become more non-additive with increasing order and molecular size/complexity.[1–4,9–13] From a theoretical point of view, an accurate and reliable description of α_ℓ can be quite demanding, and often requires sophisticated treatment of electron correlation in conjunction with large (and diffuse) basis sets.[14–19] Experimental α_ℓ measurements are also challenging and susceptible to (zero-point) vibrational contributions, thermal effects, as well as origin and orientational dependencies.[20–22]

Through the Casimir-Polder (CP) relationship,[23] the non-additivity in α_ℓ is also reflected in the dispersion coefficients (C_n), which govern the strength of the vdW forces between molecules and materials. Since even slight variations in the (effective) vdW power laws can impact the structure, stability, and properties of a system,[24–26] knowledge of how α_ℓ scales with system size is fundamental to understanding these ubiquitous non-bonded interactions. At the nanoscale, non-additivity in C_n is particularly important, as vdW forces are largely responsible for directing self-assembly and the energetic contributions from higher-order terms can be 50% of the leading-order C_6 component.[27–29] Given that fullerenes, nanotubes, and multi-layer graphene already exhibit unusual scaling behavior[24–26,30–36] at the C_6 level, enhanced non-additivity in the higher-order C_n is expected to have an even more profound effect on such nanostructures.

Of specific interest here are the fullerenes, which are characterized by quasi-spherical cage-like structures, encapsulated void spaces, and nearly uniform surface electron densities, thereby making them unique systems for studying non-additivity in the α_ℓ and C_n scaling landscapes.[24,37–40] For the popular fullerenes (*e.g.*, C_{60} and C_{70}), α_1 and C_6 have been well-investigated by theory[24,38,41–47] and experiment,[22,48–53] with most studies reporting qualitatively similar values for these leading-order terms (although direct comparison between theory and experiment has been difficult due to vibrational and thermal effects.[20–22,45,54–56]) Theoretical studies[24,38,40] have also shown that α_1 and C_6 exhibit strong non-additivity with increasing fullerene size as well as non-trivial quantum- and finite-size effects.[39,57] However, there has been little work dedicated to the higher-order α_ℓ and C_n in the fullerenes, and many existing classical models[37,58–64] for these quantities—which have largely been popularized by Tao, Perdew, and co-workers—have

* These authors contributed equally to this work.
† distasio@cornell.edu

yet to be validated using quantum mechanics and still rely on accurate α_1 (or even α_ℓ) values as input.

In this work, we address these limitations by computing *ab initio* values for the α_ℓ series ($\ell = 1, 2, 3$) in the C_{60}–C_{84} fullerenes using DFT and finite-field derivative techniques. With these values in hand, we obtain the molecular dispersion coefficients (C_n with $n = 6, 8, 9, 10$), quantitatively ascertain the intrinsic non-additivity in the α_ℓ (and C_n) series, and derive the corresponding effective scaling laws as a function of fullerene size. Detailed analysis of the *ab initio* data with respect to classical models that treat the fullerenes as conducting spherical shells or solid spheres demonstrates how the unique electronic structure of single-walled fullerenes—a complex dichotomy between electron confinement and delocalization effects—simultaneously limits and enhances their response to electric field perturbations. Analogous to the deviations from asymptotic vdW scaling laws observed at finite (nanoscale) distances, this analysis also demonstrates how quantum- and finite-size effects markedly alter the α_ℓ (and C_n) scaling landscapes in these quintessential nanostructures. We conclude this work by computing the non-negligible (≈ 1–2%) zero-point vibrational corrections[20,65–67] to α_1 for C_{60} and C_{70}, enabling a more accurate and direct comparison between experiment and theory for this fundamental response property.

RESULTS AND DISCUSSION

To begin, we computed static isotropic (electronic) polarizabilities (α_ℓ with $\ell = 1, 2, 3$) for the lowest-energy isomers of the C_{60}, C_{70}, C_{76}, C_{78}, and C_{84} fullerenes using finite-field derivatives at the SCAN0/Sadlej//SCAN0/6-31G(d) level (see the *Electronic Supplementary Information* (ESI) for computational details, Table S1 for isomer comparisons, and Tables S7–S11 for optimized structures). Since the SCAN0[68] hybrid functional, which admixes 25% exact exchange into the SCAN[69] meta-GGA functional, combined with the Sadlej[14] triple-ζ basis set, which has been optimized for molecular properties such as moments/polarizabilities, furnishes α_ℓ values to $\approx 1\%$ of benchmark quantum chemical methods for C_{20} (the smallest cage-like fullerene[70]), this level of theory was used for the larger fullerenes in this work (see Table S2). Corresponding frequency-dependent polarizabilities ($\alpha_\ell(iu)$) were obtained within the modified single-frequency approximation (MSFA)[63] by inputting α_ℓ into the hollow sphere (HS) model of Tao and Perdew,[61] and used to compute C_n ($n = 6, 8, 9, 10$) *via* the CP integral.[23] All calculations were performed using `Q-Chem`[71] and `FHI-aims`.[72]

The computed α_ℓ (and C_n) are plotted in Fig. 1 and summarized in Table I. For α_1 and C_6, our values are in excellent agreement with the available theoretical data for the fullerenes (see Table S6). In particular, we find that the SCAN0/Sadlej α_1 value for C_{60} (536.8 au) is significantly closer to the LR-CCSD/Zm3PolC value (555.3 au, with an error of 3.3%)[42] than the LR-CC2/aug-cc-pVDZ value (623.7 au).[47] Since the LR-CCSD/Zm3PolC value[42] is arguably the most accurate quantum mechanical calculation of this quantity available in the literature to date, this provides further evidence (in addition to our comparative study on C_{20} in the ESI) that SCAN0/Sadlej will offer an acceptable compromise between accuracy and feasibility when computing the higher-order multipole polarizabilities in the

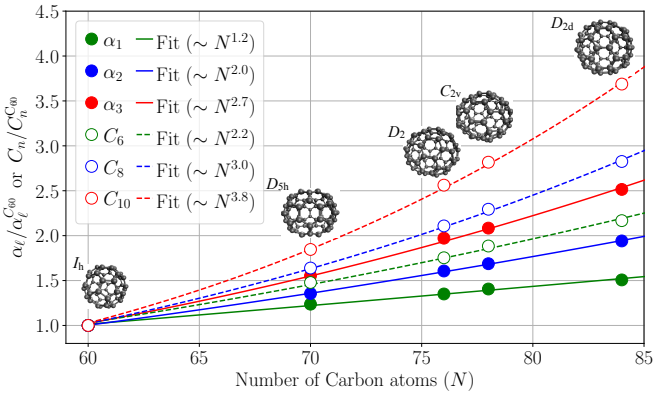

FIG. 1. Multipole polarizabilities (α_ℓ with $\ell = 1, 2, 3$) and homo-molecular dispersion coefficients (C_n with $n = 6, 8, 10$) plotted as a function of system size in the C_{60}–C_{84} fullerenes. Quantities for the larger fullerenes (C_N with $N = 70, 76, 78, 84$) are plotted relative to the corresponding C_{60} values. Also plotted are the effective scaling laws for α_ℓ (solid lines) and C_n (dashed lines), which were derived from fitting the data to a power law (aN^b) ansatz and depict the increasing non-additivity in the higher-order quantities.

TABLE I. Values (in au) for the multipole polarizabilities (α_ℓ with $\ell = 1, 2, 3$; computed at the SCAN0/Sadlej//SCAN0/6-31G(d) level) and homo-molecular dispersion coefficients (C_n with $n = 6, 8, 10$; computed by inputting α_ℓ into the HS/MSFA model) in the C_{60}–C_{84} fullerenes. Also provided are the effective scaling law parameters (and R^2 values) resulting from non-linear fits to power law (aN^b) ansätze (see Fig. 1). Higher-precision values for α_ℓ and all homo-/hetero-molecular C_n ($n = 6, 8, 9, 10$) can be found in Tables S3–S5.

	Ab Initio			*Ab Initio* + HS/MSFA		
Molecule	$\alpha_1/10^2$	$\alpha_2/10^4$	$\alpha_3/10^6$	$C_6/10^5$	$C_8/10^7$	$C_{10}/10^9$
$C_{60}(I_h)$	5.368	4.281	3.319	0.990	4.207	14.620
$C_{70}(D_{5h})$	6.638	5.800	5.150	1.462	6.891	26.963
$C_{76}(D_2)$	7.248	6.871	6.539	1.735	8.861	37.417
$C_{78}(C_{2v})$	7.542	7.217	6.910	1.863	9.639	41.138
$C_{84}(D_{2d})$	8.086	8.301	8.336	2.143	11.872	53.827
a	3.903	13.487	54.633	10.328	168.062	2505.686
b	1.206	1.970	2.696	2.246	3.041	3.812
R^2	0.994	1.000	0.998	0.996	0.999	0.999

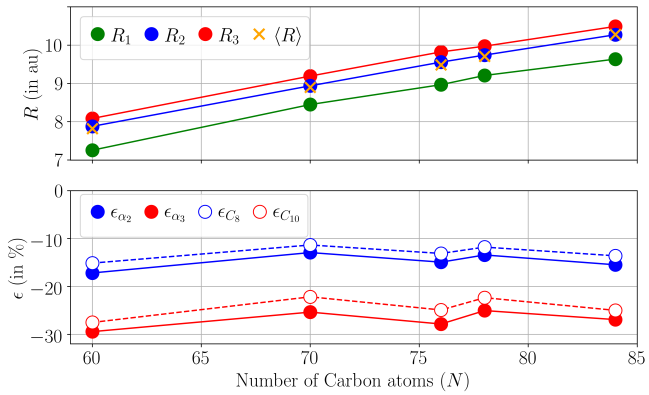

FIG. 2. *Top:* System-size dependence of the semi-classical ℓ-dependent fullerene radii (obtained using quantum mechanical α_ℓ in the classical conducting spherical shell/solid sphere model formula, $R_\ell = \alpha_\ell^{1/(2\ell+1)}$) in the C_{60}–C_{84} fullerenes. Also depicted are the corresponding estimated physical radii ($\langle R\rangle$).[74] *Bottom:* Percent errors when predicting the higher-order α_ℓ and C_n under the classical assumption of a single radius ($R = R_1$) per fullerene.

fullerenes. For the higher-order terms, α_2 and α_3 in Fig. 1 and Table I are the only *ab initio* values available to date. In previous studies,[37,40,60–64] these quantities have been estimated using a classical formula derived by Tao, Perdew, and co-workers by considering a conducting spherical shell (or solid sphere) of uniform electron density with outer radius R and thickness t, namely,[37,73]

$$\alpha_\ell \approx \alpha_\ell^{\text{model}} = R^{2\ell+1} \qquad 0 < t \leq R. \tag{1}$$

Since these are among the simplest physically sound models for the fullerenes,[37,57] we first discuss the models' assumption that α_ℓ can be derived using a single radius per fullerene by inverting this formula to obtain an ℓ-dependent radius, *i.e.*, $R_\ell = \alpha_\ell^{1/(2\ell+1)}$. These R_ℓ values—along with the estimated (outer) physical radius of each fullerene $\langle R\rangle$[74]—are plotted against N in Fig. 2. From this figure, one can see that $R_1 \approx R_2 \approx R_3 \approx \langle R\rangle$ for C_{60}–C_{84}; with mean signed deviations of -2.9% (R_1), $+0.2\%$ (R_2), and $+1.5\%$ (R_3), each R_ℓ agrees fairly well with $\langle R\rangle$, and the emerging picture is, as expected, qualitatively consistent with these classical models. In the same data, we also observe a weak (but still increasing) dependence of R_ℓ on ℓ as $R_3 \gtrsim R_2 \gtrsim R_1$ for each fullerene. Here, we argue that both of these observations can be rationalized by considering the unique electronic structure of the fullerenes, whose quasi-spherical cage-like structures and encapsulated void spaces lead to an essentially metallic electron density that is delocalized across the entire fullerene surface, yet largely confined to a thin surrounding shell. Unlike the classical spherical shell and solid sphere models—in which the density is confined to an infinitesimally thin shell surrounding the conductor[37]—surface electrons on the fullerenes still retain some degree of radial flexibility, which serves to *enhance* their (relative) response to electric field perturbations. This property manifests itself in the (albeit weak) growth of R_ℓ with ℓ observed above, which indicates enhanced non-additivity in the fullerenes beyond that due to the increasingly higher-order powers in the classical α_ℓ formula. In the same breath, the fact that the electrons on the fullerene surface are largely confined to a surrounding thin shell also simultaneously *limits* the radial extent of their quantum mechanical response to external electric fields. Evidence of this is seen in the qualitatively similar R_ℓ values in Fig. 2 that only weakly depend on ℓ; although higher-order α_ℓ data is scarce, the dependence of R_ℓ on ℓ seems to be stronger for extended molecular systems like n-alkanes,[75] and is expected to be even more pronounced in conjugated systems like s-*trans* alkenes and polyacenes.[76]

Although the differences among R_ℓ seem small, the errors made when predicting α_ℓ (and C_n) under the classical assumption of a single radius per fullerene can be substantial and warrant further discussion. Since an accurate determination of α_1 is most straightforward among the α_ℓ series, we first set $R = R_1 = \alpha_1^{1/3}$ for each fullerene (following previous work in Refs.[40,60,62–64,73]) and re-compute α_2 and α_3 *via* the classical formula, $\alpha_\ell \approx \alpha_\ell^{\text{model}} = R^{2\ell+1}$. The corresponding errors, $\epsilon_{\alpha_\ell} \equiv (\alpha_\ell^{\text{model}} - \alpha_\ell)/\alpha_\ell$, are also plotted in Fig. 2, from which one can immediately see that these higher-order properties are substantially *underestimated* in C_{60}–C_{84}. With mean deviations of $14.8 \pm 1.5\%$ (α_2) and $26.9 \pm 1.6\%$ (α_3), these errors are significant in magnitude and increase with ℓ; such discrepancies can be traced back to the variability in R_ℓ (*e.g.*, $R_3 \gtrsim R_2 \gtrsim R_1$), which becomes amplified by the increasingly higher-order powers in the classical formula. Also depicted are the errors which propagate into C_8 and C_{10} when inputting these α_ℓ values into the HS/MSFA model; with mean deviations of $13.0\pm1.3\%$ (C_8) and $24.4\pm2.0\%$ (C_{10}), the non-additivity in these quantities is also substantially underestimated, rendering them unsuitable for describing the non-trivial vdW interactions between fullerenes. Here, the errors in C_8 and C_{10} are quite similar to those in α_2 and α_3, which follows from factoring α_ℓ out of the CP integral (which yields $C_8 \propto \alpha_1\alpha_2$ and $C_{10} \propto \alpha_1\alpha_3 + \alpha_2\alpha_2$).[40,61] We further note that the R values used to generate the error profile in Fig. 2 are not unique. Setting $R = \langle R\rangle$ is also physically justifiable, and overestimates α_1 by 9.4% and underestimates α_2 and α_3 by 1.0% and 9.9%, respectively;[77] since $\langle R\rangle \approx R_2$, the error is still substantial and simply redistributed onto α_1 and α_3. Another logical choice for R arises from treating each fullerene as a spherical dielectric shell[78] with ε derived from the HOMO–LUMO gap.[57,79] For C_{60}, this yields an R that is only 1.5% larger than R_1 and hence a similar error profile to that in Fig. 2; this also demonstrates that the models' assumption that each fullerene is metallic is far less

important than the classical single-radius approximation. Connections to modern vdW radii theory[80,81] might also be interesting to consider here.

As the system size increases, the error introduced by using a single radius to predict α_2 and α_3 (or C_8 and C_{10}) is fairly constant and does not increase with N (see Fig. 2). Such system-size-independent deviations are reflected in the relatively small ($\approx 1.5\%$) standard deviations in ϵ_{α_ℓ} (and ϵ_{C_n}), and are primarily due to the fact that the variability among R_ℓ values also does not increase with N for C_{60}–C_{84} (*cf.* $R_2/R_1 = 1.04$ (1.03) versus $R_3/R_1 = 1.05$ (1.05) for C_{60} (C_{84})). Physically speaking, this can be attributed to the unique topology of the fullerenes, in which the electron density is largely confined to a thin shell whose thickness does not grow with N;[40,57,63] as discussed above, this limits the radial extent of the fullerene quantum mechanical response and suppresses the growth of R_ℓ with ℓ. Since this salient feature of the fullerenes can be qualitatively captured using a single radius (per fullerene), the classical spherical shell and solid sphere models are able to qualitatively account for the system-size dependence of α_ℓ (and C_n) in C_{60}–C_{84}. In the same breath, one can also attribute these system-size-independent deviations to the models' treatment of each fullerene as a single object instead of a collection of atoms;[63] in doing so, many-body interactions and electron delocalization effects—both of which are size-dependent, quantum mechanical in nature, and largely responsible for the non-additivity in these quantities—are also partially accounted for by these classical models. Quantitatively speaking, the classical approximation of a *single radius* per fullerene is simply not flexible enough for an accurate prediction of α_ℓ and C_n; when computing C_n (in particular), more sophisticated models that account for the non-trivial ℓ-dependence of R_ℓ (*e.g.*, HS/MSFA[61,63])—in conjunction with the high-quality *ab initio* α_ℓ values provided herein—are crucial for an accurate and reliable description of any vdW interactions involving these quintessential nanostructures.

To further explore how α_ℓ (and C_n) scale with fullerene size, we now derive the corresponding effective scaling laws by fitting our data to power law (aN^b) ansätze. The fitted functions are plotted in Fig. 1, and the resulting parameters (and R^2 values) are provided in Table I. With $R^2 > 0.99$ in all cases, these fits accurately describe the system-size dependence in these quantities, yielding negligible fitting errors of -0.04%, -0.02%, -0.22% for $\alpha_1, \alpha_2, \alpha_3$ (-0.21%, -0.22%, -0.38% for C_6, C_8, C_{10}). Here, we find that α_1, α_2, and α_3 scale as $\sim N^{1.2}$, $\sim N^{2.0}$, and $\sim N^{2.7}$ for the C_{60}–C_{84} fullerenes; with exponents that substantially deviate from unity, these quantities are all strongly non-additive and become increasingly more so for larger ℓ. For α_1, our finding that $b = 1.21$ is in excellent agreement with the TD-DFT results of Kauczor *et al.* ($b = 1.25$)[38] (see Table II); here, we note that the b values obtained from aN^b fits of the TD-HF, TD-B3LYP, and TD-CAM-B3LYP data in Ref.[38] are all within 1%−2% of the SCAN0/Sadlej value, which suggests that the non-additivity in α_1 is largely independent of the underlying exchange-correlation functional. Due to the scarcity of higher-order α_ℓ, the b values obtained herein for α_2 and α_3 are the only *ab initio* values available to date. We note in passing that comparisons to the values provided by Saidi *et al.*[39] and Tao *et al.*[40] would not be appropriate, as these values correspond to a much wider range of finite-sized fullerenes (*e.g.*, C_{60}–C_{720}[39] and C_{60}–C_{3840}.[40]) Furthermore, we stress that the value of b can largely depend on the choice of ansatz and the fitting procedure, wherein one can expect some variability in the results obtained using the single-parameter N^b ansatz employed by Kauczor *et al.*,[38] and significantly larger variability when using the two-point ($\alpha_\ell^A/N_A = \alpha_\ell^B/N_B^b$) formula employed by Tao *et al.*[40]

TABLE II. Effective scaling law exponents (b) for the polarizabilities (α_ℓ) and dispersion coefficients (C_n) in the fullerenes.

	α_1	α_2	α_3	C_6	C_8	C_{10}
Ab Initio[a]	1.21[b]	1.97[b]	2.70[b]	–	–	–
Ab Initio + HS/MSFA[a]	–	–	–	2.25[b]	3.04[b]	3.81[b]
$N \propto R^2$ (spherical shell)[c]	1.50[b]	2.50[b]	3.50[b]	2.75[d]	3.75[d]	4.75[d]
$N \propto R^3$ (solid sphere)[e]	1.00[b]	1.67[b]	2.33[b]	2.00[d]	2.67[d]	3.33[d]
Gobre *et al.*[24f]	–	–	–	2.25	–	–
Kauczor *et al.*[38g]	1.25	–	–	2.19	–	–
Saidi *et al.*[39h]	1.46	–	–	2.80	–	–
Tao *et al.*[40i]	1.19	1.65	2.11	2.26	2.73	3.20

[a] C_{60}–C_{84}. [b] This work. [c] Classical conducting spherical shell model; $R \to \infty$ limit. [d] Ref.[37]. [e] Classical conducting solid sphere model; all R values. [f] Self-consistent screening (SCS) model; C_{20}–C_{540}. [g] Time-dependent DFT (B3LYP); N^b fit for C_{60}–C_{84}. [h] Capacitance-polarizability interaction (CPI) model; C_{60}–C_{720}. [i] Two-point formula ($\alpha_\ell^A/N_A = \alpha_\ell^B/N_B^b$) based on approximate α_ℓ (and C_n) for C_{60} and C_{3840}.

To characterize how finite-size effects influence the α_ℓ (and C_n) scaling landscape for C_{60}–C_{84}, we therefore discuss our findings with respect to the formal ($R \to \infty$) limits of the classical conducting spherical shell and solid sphere models. Since $N \propto R^2$ for a spherical shell (in the $R \to \infty$ limit) and $N \propto R^3$ for a solid sphere (for all R values), these models agree in how α_ℓ grows with R, but differ in how α_ℓ grows with N, *i.e.*, $\alpha_\ell = R^{2\ell+1} = N^{(2\ell+1)/\delta}$ with $\delta = 2$ (spherical shell) and $\delta = 3$ (solid sphere). The corresponding scaling law exponents for α_ℓ (and C_n) based on these models are provided in Table II, from which one can see that the growth of α_ℓ with N for a classical solid sphere conductor is slower than that in the C_{60}–C_{84} fullerenes, which in turn is markedly slower than that predicted by the $R \to \infty$ limit of the spherical shell model. Again, both of these observations can be rationalized by considering the dichotomous electronic structure of the finite-sized fullerenes, wherein a complex interplay between electron confinement and delocalization governs their quantum mechanical response to electric field perturbations. On one hand, confinement of the electrons to a thin shell unusually far from the fullerene center leads to a substantially more polarizable electron

density than the distribution of the same number of electrons throughout the volume of a solid sphere (with a necessarily smaller R), thereby leading to enhanced α_ℓ values compared to the classical solid sphere model. On the other hand, the curvature in the finite-sized fullerenes (due to their encapsulated void spaces) suppresses many-body polarization[26] of the electrons across the surface, which limits the extent of the electronic response and leads to reduced α_ℓ values compared to the graphene-like $R \to \infty$ limit of the classical spherical shell model. As such, finite-size effects have a marked impact on the growth of α_ℓ with N in the C_{60}–C_{84} fullerenes, and are analogous to the distance-dependent effective vdW power laws observed in both finite and extended systems across the nanoscale.[25,26,30–36,82]

With α_1 values in hand, finite-size effects in the effective power laws for α_2 and α_3 can be approximately accounted for (to within 1%–2%) by fitting the corresponding semi-classical α_ℓ values ($\alpha_\ell = R^{2\ell+1}$ with $R = R_1 = \alpha_1^{1/3}$) to the aN^b ansatz. As described above, this finding is reflected in the system-size-independent error profile in Fig. 2, and largely follows from the models' holistic treatment of each fullerene as a molecule (instead of a collection of atoms) with a fixed radius. Hence, the rather sizable errors in α_2 and α_3 depicted in Fig. 2 primarily result from a marked ($\approx$ 20%–40%) difference in the a values obtained with *ab initio* and classical treatments of the C_{60}–C_{84} fullerenes, and are therefore indicative of a substantial quantum-size effect on the power law pre-factor.

For the C_n, we find that C_6, C_8, and C_{10} scale as $\sim N^{2.2}$, $\sim N^{3.0}$, and $\sim N^{3.8}$, which is again indicative of strong non-additivity that increases with ℓ (and n). Since this non-additivity primarily originates from the intrinsic non-additivity in the underlying α_ℓ, our discussion of the C_n scaling laws will be brief. For C_6, our finding that $b = 2.25$ is in excellent agreement with previous studies employing time-dependent DFT ($b = 2.19$)[38] (see Table II); due to the scarcity of higher-order C_n, the b values obtained herein for C_8 and C_{10} in C_{60}–C_{84} are the only *ab initio* values available to date (and even these values still rely on the HS/MSFA model for the frequency dependence of the underlying polarizabilities). Following the analysis performed above for α_ℓ, we again find that our results lie between the $N^{n/3}$ and $N^{(n-1/2)/2}$ dependence of the solid sphere and spherical shell models;[37] as such, our data unambiguously confirms that the C_n in C_{60}–C_{84} grow much faster than a pairwise-additive model (like the classical solid sphere model) would suggest.

Returning to the *ab initio* α_ℓ provided herein, we conclude this work by investigating the zero-point vibrational contributions (zpvc) to α_1 in the popular C_{60} and C_{70} fullerenes, as these often non-negligible contributions enable a more direct comparison between experiment and theory. For a molecule in its ground vibrational state, α_1^{zpvc} can be computed using first-order perturbation theory[65–67] as $\alpha_1^{\text{zpvc}} = \sum_i \kappa_i$, in which

$$\kappa_i \equiv \frac{1}{4}\left[\left(\frac{\partial^2 \alpha_1}{\partial q_i^2}\right)_0 - \sum_j \frac{\phi_{iij}}{\omega_j}\left(\frac{\partial \alpha_1}{\partial q_j}\right)_0\right], \qquad (2)$$

is the contribution from the i-th vibrational mode. In this expression, $(\partial^n \alpha_1/\partial q_j^n)_0$ are the n-th partial derivatives of α_1 (evaluated at the equilibrium structure) with respect to (dimensionless) normal mode q_j with frequency ω_j, ϕ_{iij} are the anharmonic (cubic) force constants, and the sum includes all vibrational modes; see ESI and Ref.[18] for more details. To obtain *ab initio* values for these quantities, we performed an extensive series of (>140,000) DFT calculations, and found that $\alpha_1^{\text{zpvc}} = 8.5$ au (C_{60}) and 9.6 au (C_{70}); these vibrational contributions are non-negligible in magnitude and account for $\approx$ 1.6% and $\approx$ 1.4% of α_1. Individual contributions (κ_i) to α_1^{zpvc} from each vibrational mode in C_{60} are plotted in Fig. 3. Similar to α_1^{zpvc} in water,[18] the primary vibrational contributions are due to high-frequency bond-stretching modes;[83] (*i.e.*, $\approx$ 1400–1600 cm^{-1} largest contribution from the H_u mode at $\omega = 1564$ cm^{-1}), and not low-frequency squashing ($\approx$ 250 cm^{-1}) and/or breathing ($\approx$ 500 cm^{-1}) modes.[84–86] From Table III, one can see that our (electronic) α_1 value is slightly smaller than the DOSD estimate[22,52] for C_{60}, while $\alpha_1^{\text{tot}} = \alpha_1 + \alpha_1^{\text{zpvc}}$ are well within the error bars measured by molecular beam deflection[48,50] and time-of-flight spectrometry[49] for C_{60} and C_{70}. While our values are consistently smaller than those obtained using matter-wave interferometry,[51,53] the experimental ratios of $\alpha_1^{\text{tot,C}_{70}}/\alpha_1^{\text{tot,C}_{60}} = 1.22$ (believed to be more accurate than the absolute α_1 values) using this technique are in excellent agreement with our *ab initio* ratio of 1.23. Although not directly comparable to the α_1^{zpvc} values computed herein, we note in passing that previous theoretical estimates (in the double-harmonic approximation) of α_1^v in C_{60}, *i.e.*, the so-called "pure vi-

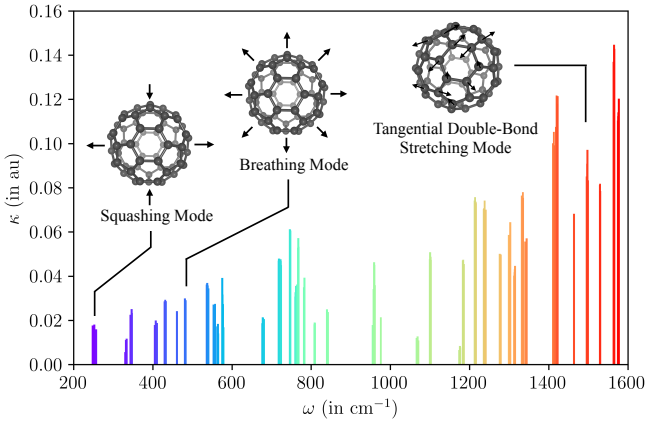

FIG. 3. Individual mode contributions (κ in au) to α_1^{zpvc} in C_{60} (computed at the SCAN/tier-1//SCAN/tier-1 level). The corresponding plot for C_{70} is provided in Fig. S1.

TABLE III. Summary of the *ab initio* electronic (α_1, computed at the SCAN0/Sadlej//SCAN0/6-31G(d) level), zero-point vibrational (α_1^{zpvc}, computed at the SCAN/tier-1//SCAN/tier-1 level), and total ($\alpha_1^{\text{tot}} \equiv \alpha_1 + \alpha_1^{\text{zpvc}}$) polarizabilities for C_{60} and C_{70} along with the available experimental data.

	Theory			Experiment
	α_1	α_1^{zpvc}	α_1^{tot}	α_1^{tot}
C_{60}	536.8	8.5	545.3	516.2±54[a], 533.1±27[b], 599.9±41[c] 558.6±17[d], 589.8±20[e]
C_{70}	663.8	9.6	673.4	688.3±95[f], 732.2±55[c], 718.0±9[e]

[a]Molecular beam deflection.[48] [b]Time-of-flight spectrometry.[49] [c]Matter-wave interferometry.[51] [d]Dipole oscillator strength distribution (DOSD) estimate of α_1.[22,52] [e]Matter-wave interferometry.[53] [f]Molecular beam deflection.[50]

brational" contribution to α_1,[67,87] ranged from 3.9 au[56] to 5.3 au;[45] this higher-order term accounts for vibrational effects beyond α_1^{zpvc} and should be included when comparing to experimental α_1 values determined at finite frequencies. Furthermore, we also note that experimental estimates for the vibrational contributions to α_1 in C_{60} (*i.e.*, including α_1^{zpvc} and higher-order terms) have been obtained for the C_{60} molecular crystal and range from 2.5 au and 8.4 au[54] to 13.5 au.[55]

CONCLUSIONS

In conclusion, the α_ℓ (and C_n) provided herein for C_{60}–C_{84} are the most accurate and reliable theoretical values obtained to date, and unequivocally demonstrate that these quantities are strongly non-additive and become increasingly more so for larger ℓ (and n). Derivation of the corresponding effective scaling laws in addition to a critical analysis of the α_ℓ and C_n data in the context of the classical spherical shell and solid sphere models provides new insight into how the unique electronic structure of the single-walled fullerenes—a complex interplay between electron confinement effects and charge delocalization due to the structure and topology of these nanosystems—serves to both limit and enhance their response to electric field perturbations. Of particular interest are the quantum- and finite-size effects observed in these scaling laws, which are analogous (and intimately related) to the deviations from asymptotic vdW scaling laws observed in both finite and extended systems at nanoscale distances,[25,26,30–36,82] and undoubtedly impact the structure, function, and properties of these quintessential nanostructures.

ACKNOWLEDGMENTS

All authors acknowledge helpful scientific discussions with Hsin-Yu Ko, Alexandre Tkatchenko, and Yang Yang. This work was primarily supported by the Cornell Center for Materials Research with funding from the NSF MRSEC program (DMR-1719875). This research used resources of the National Energy Research Scientific Computing Center, which is supported by the Office of Science of the U.S. Department of Energy under Contract No. DE-AC02-05CH11231. This research used resources of the Argonne Leadership Computing Facility at Argonne National Laboratory, which is supported by the Office of Science of the U.S. Department of Energy under Contract No. DE-AC02-06CH11357.

1 K. D. Bonin and V. V. Kresin, *Electric-Dipole Polarizabilities of Atoms, Molecules, and Clusters*, World Scientific, Singapore, 1997.
2 G. Maroulis, *Atoms, Molecules and Clusters in Electric Fields: Theoretical Approaches to the Calculation of Electric Polarizability*, World Scientific, Singapore, 2006.
3 G. Maroulis, *Computational Aspects of Electric Polarizability Calculations: Atoms, Molecules and Clusters*, IOS Press, Amsterdam, 2006.
4 A. J. Stone, *The Theory of Intermolecular Forces*, Oxford University Press, Oxford, 2nd edn, 2013.
5 S. Grimme, A. Hansen, J. G. Brandenburg and C. Bannwarth, *Chem. Rev.*, 2016, **116**, 5105–5154.
6 J. Hermann, R. A. DiStasio Jr. and A. Tkatchenko, *Chem. Rev.*, 2017, **117**, 4714–4758.
7 S. Luber, M. Iannuzzi and J. Hutter, *J. Chem. Phys.*, 2014, **141**, 094503.
8 G. R. Medders and F. Paesani, *J. Am. Chem. Soc.*, 2016, **138**, 3912–3919.
9 H.-Y. Kim, J. O. Sofo, D. Velegol, M. W. Cole and G. Mukhopadhyay, *Phys. Rev. A*, 2005, **72**, 053201.
10 H.-Y. Kim, J. O. Sofo, D. Velegol, M. W. Cole and A. A. Lucas, *J. Chem. Phys.*, 2006, **124**, 074504.
11 A. Mayer, *Phys. Rev. B*, 2007, **75**, 045407.
12 H.-Y. Kim, J. O. Sofo, D. Velegol, M. W. Cole and A. A. Lucas, *Langmuir*, 2007, **23**, 1735–1740.
13 T. Helgaker, S. Coriani, P. Jørgensen, K. Kristensen, J. Olsen and K. Ruud, *Chem. Rev.*, 2012, **112**, 543–631.
14 A. J. Sadlej, *Collect. Czech. Chem. Commun.*, 1988, **53**, 1995–2016.
15 D. E. Woon and T. H. Dunning Jr., *J. Chem. Phys.*, 1994, **100**, 2975–2988.
16 J. R. Hammond, W. A. de Jong and K. Kowalski, *J. Chem. Phys.*, 2008, **128**, 224102.
17 J. R. Hammond, N. Govind, K. Kowalski, J. Autschbach and S. S. Xantheas, *J. Chem. Phys.*, 2009, **131**, 214103.
18 K. U. Lao, J. Jia, R. Maitra and R. A. DiStasio Jr., *J. Chem. Phys.*, 2018, **149**, 204303.
19 Y. Yang, K. U. Lao, D. M. Wilkins, A. Grisafi, M. Ceriotti and R. A. DiStasio Jr., *Sci. Data*, 2019, **6**, 152.
20 D. M. Bishop, *Rev. Mod. Phys.*, 1990, **62**, 343–374.
21 S. Kümmel, J. Akola and M. Manninen, *Phys. Rev. Lett.*, 2000, **84**, 3827–3830.
22 U. Hohm, *J. Mol. Struct.*, 2013, **1054**, 282–292.
23 H. B. G. Casimir and B. Polder, *Phys. Rev.*, 1948, **73**, 360–372.
24 V. V. Gobre and A. Tkatchenko, *Nat. Commun.*, 2013, **4**, 2341.
25 A. Ambrosetti, N. Ferri, R. A. DiStasio Jr. and A. Tkatchenko, *Science*, 2016, **351**, 1171–1176.

26 Y. Yang, K. U. Lao and R. A. DiStasio Jr., *Phys. Rev. Lett.*, 2019, **122**, 026001.
27 E. R. Johnson and A. D. Becke, *J. Chem. Phys.*, 2006, **124**, 174104.
28 J. Tao, J. P. Perdew and A. Ruzsinszky, *Phys. Rev. B*, 2010, **81**, 233102.
29 J. Tao, J. Yang and A. M. Rappe, *J. Chem. Phys.*, 2015, **142**, 164302.
30 T. Gould, K. Simpkins and J. F. Dobson, *Phys. Rev. B*, 2008, **77**, 165134.
31 L. Spanu, S. Sorella and G. Galli, *Phys. Rev. Lett.*, 2009, **103**, 196401.
32 Y. J. Dappe, J. Ortega and F. Flores, *Phys. Rev. B*, 2009, **79**, 165409.
33 S. Lebègue, J. Harl, T. Gould, J. G. Ángyán, G. Kresse and J. F. Dobson, *Phys. Rev. Lett.*, 2010, **105**, 196401.
34 A. J. Misquitta, J. Spencer, A. J. Stone and A. Alavi, *Phys. Rev. B*, 2010, **82**, 075312.
35 A. J. Misquitta, R. Maezono, N. D. Drummond, A. J. Stone and R. J. Needs, *Phys. Rev. B*, 2014, **89**, 045140.
36 P. S. Venkataram, J. Hermann, A. Tkatchenko and A. W. Rodriguez, *Phys. Rev. Lett.*, 2017, **118**, 266802.
37 A. Ruzsinszky, J. P. Perdew, J. Tao, G. I. Csonka and J. M. Pitarke, *Phys. Rev. Lett.*, 2012, **109**, 233203.
38 J. Kauczor, P. Norman and W. A. Saidi, *J. Chem. Phys.*, 2013, **138**, 114107.
39 W. A. Saidi and P. Norman, *J. Chem. Phys.*, 2016, **145**, 024311.
40 J. Tao, Y. Jiao, Y. Mo, Z. H. Yang, J. X. Zhu, P. Hyldgaard and J. P. Perdew, *Phys. Rev. B*, 2018, **97**, 155143.
41 A. Jiemchooroj, P. Normana and B. E. Sernelius, *J. Chem. Phys.*, 2005, **123**, 124312.
42 K. Kowalski, J. R. Hammond, W. A. de Jong and A. J. Sadlej, *J. Chem. Phys.*, 2008, **129**, 226101.
43 D. H. Friese, N. O. C. Winter, P. Balzerowski, R. Schwan and C. Hättig, *J. Chem. Phys.*, 2012, **136**, 174106.
44 P. Giannozzi and S. Baroni, *J. Chem. Phys.*, 1994, **100**, 8537–8539.
45 E. A. Perpète, B. Champagne and B. Kirtman, *Phys. Rev. B*, 2000, **61**, 13137–13141.
46 K. Ruud, D. Jonsson and P. R. Taylor, *J. Chem. Phys.*, 2001, **114**, 4331–4332.
47 T. B. Pedersen, A. M. J. Sánchez de Merás and H. Koch, *J. Chem. Phys.*, 2004, **120**, 8887–8897.
48 R. Antoine, Ph. Dugourd, D. Rayane, E. Benichou and M. Broyer, *J. Chem. Phys.*, 1999, **110**, 9771–9772.
49 A. Ballard, K. Bonin and J. Louderback, *J. Chem. Phys.*, 2000, **113**, 5732–5735.
50 I. Compagnon, R. Antoine, M. Broyer, Ph. Dugourd, J. Lermé and D. Rayane, *Phys. Rev. A*, 2001, **64**, 025201.
51 M. Berninger, A. Stefanov, S. Deachapunya and M. Arndt, *Phys. Rev. A*, 2007, **76**, 013607.
52 A. Kumar and A. J. Thakkar, *Chem. Phys. Lett.*, 2011, **516**, 208–211.
53 Y. Y. Fein, P. Geyer, F. Kiałka, S. Gerlich and M. Arndt, *Phys. Rev. Res.*, 2019, **1**, 033158.
54 G. Gensterblum, Y. Li-Ming, J.-J. Pireaux, P. A. Thiry, R. Caudano, Ph. Lambin, A. A. Lucas, W. Krätschmer and J. E. Fischer, *J. Phys. Chem. Solids*, 1992, **53**, 1427–1432.
55 P. C. Eklund, A. M. Rao, Y. Wang, P. Zhou, K. A. Wang, J. M. Holden, M. S. Dresselhaus and G. Dresselhaus, *Thin Solid Films*, 1995, **257**, 211–232.
56 M. R. Pederson, T. Baruah, P. B. Allen and C. Schmidt, *J. Chem. Theory Comput.*, 2005, **1**, 590–596.
57 G. K. Gueorguiev, J. M. Pacheco and D. Tománek, *Phys. Rev. Lett.*, 2004, **92**, 215501.
58 A. A. Lucas, L. Henrard and Ph. Lambin, *Phys. Rev. B*, 1994, **49**, 2888–2896.
59 J. Tao, J. P. Perdew and A. Ruzsinszky, *Proc. Natl. Acad. Sci. USA*, 2012, **109**, 18–21.
60 J. P. Perdew, J. Tao, P. Hao, A. Ruzsinszky, G. I. Csonka and J. M. Pitarke, *J. Phys. Condens. Matter*, 2012, **24**, 424207.
61 J. Tao and J. P. Perdew, *J. Chem. Phys.*, 2014, **141**, 141101.
62 J. Tao, Y. Fang, P. Hao, G. E. Scuseria, A. Ruzsinszky and J. P. Perdew, *J. Chem. Phys.*, 2015, **142**, 024312.
63 J. Tao, Y. Mo, G. Tian and A. Ruzsinszky, *Phys. Rev. B*, 2016, **94**, 085126.
64 J. Tao and A. M. Rappe, *J. Chem. Phys.*, 2016, **144**, 031102.
65 P. W. Fowler, *Mol. Phys.*, 1981, **43**, 591–600.
66 P. W. Fowler, *Mol. Phys.*, 1984, **51**, 1423–1428.
67 A. J. Russell and M. A. Spackman, *Mol. Phys.*, 1995, **84**, 1239–1255.
68 K. Hui and J.-D. Chai, *J. Chem. Phys.*, 2016, **144**, 044114.
69 J. Sun, A. Ruzsinszky and J. P. Perdew, *Phys. Rev. Lett.*, 2015, **115**, 036402.
70 H. Prinzbach, A. Weiler, P. Landenberger, F. Wahl, J. Wörth, L. T. Scott, M. Gelmont, D. Olevano and B. von Issendorff, *Nature*, 2000, **407**, 60–63.
71 Y. Shao *et al.*, *Mol. Phys.*, 2015, **113**, 184–215.
72 V. Blum, R. Gehrke, F. Hanke, P. Havu, V. Havu, X. Ren, K. Reuter and M. Scheffler, *Comput. Phys. Commun.*, 2009, **180**, 2175–2196.
73 J. P. Perdew, A. Ruzsinszky, J. Sun, S. Glindmeyer and G. I. Csonka, *Phys. Rev. A*, 2012, **86**, 062714.
74 The outer physical radius was estimated *via* $\langle R\rangle = \langle r\rangle + t/2$, in which $\langle r\rangle$ is the average distance from each atom to the nuclear center of charge and $t = 3.4$ Bohr[57,58].
75 G. F. Thomas, F. Mulder and W. J. Meath, *Chem. Phys.*, 1980, **54**, 45–54.
76 D. M. Wilkins, A. Grisafi, Y. Yang, K. U. Lao, R. A. DiStasio Jr. and M. Ceriotti, *Proc. Natl. Acad. Sci. USA*, 2019, **116**, 3401–3406.
77 For C_n, the choice of $R = \langle R\rangle$ overestimates C_6 and C_8 by 14.2% and 5.7%, and underestimates C_{10} by 2.4%.
78 Ph. Lambin, A. A. Lucas and J.-P. Vigneron, *Phys. Rev. B*, 1992, **46**, 1794–1803.
79 D. R. Penn, *Phys. Rev.*, 1962, **128**, 2093–2097.
80 M. Rahm, R. Hoffmann and N. W. Ashcroft, *Chem. Eur. J.*, 2016, **22**, 14625–14632.
81 D. V. Fedorov, M. Sadhukhan, M. Stöhr and A. Tkatchenko, *Phys. Rev. Lett.*, 2018, **121**, 183401.
82 K. A. Makhnovets and A. K. Kolezhuk, *Phys. Rev. B*, 2017, **96**, 125427.
83 L. T. Chadderton, *J. Phys. Chem. Solids*, 1993, **54**, 1027–1033.
84 H.-J. Eisler, S. Gilb, F. H. Hennrich and M. M. Kappes, *J. Phys. Chem. A*, 2000, **104**, 1762–1768.
85 H.-J. Eisler, F. H. Hennrich, S. Gilb and M. M. Kappes, *J. Phys. Chem. A*, 2000, **104**, 1769–1773.
86 D. Jing and Z. Pan, *Eur. J. Mech. A-Solid*, 2009, **28**, 948–954.
87 J. Martí and D. M. Bishop, *J. Chem. Phys.*, 1993, **99**, 3860–3864.